FEATURE ARTICLE

Reaction Kinetics on Complex Model Catalysts under Single Scattering Conditions

J. Libuda* and H.-J. Freund

Fritz-Haber-Institut der Max-Planck-Gesellschaft, Faradayweg 4-6, 14195 Berlin, Germany

Received: November 5, 2001; In Final Form: February 20, 2002

To approach a microscopic understanding of the reaction kinetics on complex surfaces of heterogeneous catalysts, we combine multimolecular beam techniques and a supported model catalyst approach. The model systems are prepared under ultrahigh vacuum (UHV) conditions and have been characterized in detail with respect to their geometric and electronic structure. To probe the kinetics of catalytic reactions on these systems, we have developed a molecular beam instrument, which allows us to cross up to three beams on the sample surface. The simultaneous detection of reaction products and surface species is established by a combination of angle- and time-resolved gas-phase detection and in situ time-resolved IR reflection absorption spectroscopy. In this paper, we review a variety of representative experiments, illustrating the experimental possibilities of the molecular beam approach. As a model surface, we focus on alumina supported palladium particles. We cover the adsorption and desorption kinetics of small molecules and the kinetics of simple surface reactions on these systems. The reaction kinetics is probed via systematic steady state measurements, transient experiments, time-resolved in situ IR spectroscopy and measurements of the angular distribution of products. A central topic is the CO oxidation, a model reaction, which has been thoroughly investigated on a variety of single crystal surfaces. For the supported model catalysts, it is shown how structure and size dependencies can be identified by performing systematic kinetic measurements. These effects can be linked to the inherent heterogeneity of the model surfaces via microkinetic mean-field and Monte Carlo simulations. It is shown that the particular kinetic effects on the model catalyst surfaces can be understood by explicitly accounting for their inherent complexity. Finally, we outline possible future directions of the molecular beam approach applied to complex model surfaces.

1. Introduction

Most of the heterogeneous catalysts commercially applied, e.g., in chemical synthesis or environmental applications are highly complex systems, both with respect to their structural properties and composition (see, e.g., ref 1). Selectivities and activities of such systems often depend in a highly sensitive and only poorly understood way on their geometric and electronic structure, the role promoters and poisons, or the interplay between different functionalities simultaneously present on a surface.

Motivated by the outstanding importance of heterogeneously catalyzed processes, an improved microscopic understanding of underlying reaction kinetics would be highly desirable. If we would like to approach a microscopic understanding of reaction kinetics on this type of complex surfaces, however, we are facing two problems that need to be solved simultaneously:

The first problem arises as a consequence of the vast complexity of real catalysts and is frequently denoted as the *materials* gap (see, e.g., refs 2 and 3) between surface science and catalysis. The difficulties related to the *complexity* of real catalytic materials are made even more severe by the fact that the experimental accessibility of these systems to many surface science techniques is rather limited, e.g., as a consequence of the microporousity and limited electrical conductivity of commonly used catalyst supports. In most cases, these difficulties have prevented a detailed understanding of the underlying reaction mechanisms and kinetics. Single crystals, on the other hand, are easily accessible experimentally and for some reaction systems the kinetics can be successfully reproduced on such simple surfaces. As soon as modifications of the kinetics arise from the complexity of the catalyst, however, they will necessarily fail to reproduce these effects.[4,5]

As a strategy to overcome this problem, model surfaces have been developed. These model systems allow us to introduce certain complex aspects of the real catalyst surface in a well-controlled manner and still remain easily accessible for surface science experiments. For supported catalysts for example, a variety of model systems has been developed, using both oxide single crystals (see ref 6 and references therein) and thin oxide films[3,7−9] as supports. In this work, we will employ supported model catalysts, which are based on a thin ordered alumina film, which has been characterized with respect to its geometric and electronic structure.[10,11] To build a metal/alumina model system, the active metal particles are prepared by UHV deposition under

* Corresponding author. E-mail: libuda@fhi-berlin.mpg.de. FAX: +49-30-8413-4309.

10.1021/jp014055e CCC: $22.00
Published on Web 05/09/2002

well-controlled conditions.[3,7,12,13] As has been shown previously,[7,13] structure, density, and size of these particles can be controlled over a wide range via choosing the appropriate preparation conditions.

The second problem, commonly denoted as the so-called *pressure gap*, is related to the fact that catalytic processes are typically run under high pressure and high throughput conditions. In surface science, on the other hand, most experimental techniques giving access to reaction kinetics and mechanisms rely on temperature controlled desorption and reaction techniques in a UHV environment. These techniques have been highly successful with respect to the analysis of reaction mechanisms and kinetics. However, there are also problems connected with these experimental conditions: First, it has to be verified that the results obtained under UHV conditions are relevant for higher pressure conditions. Second, while temperature programmed techniques very efficiently provide qualitative information on a surface reaction, detailed and quantitative kinetics are sometimes difficult to extract and require series of highest quality experiments.

Clearly, it is desirable to provide a kinetic probe, which connects the quantitative kinetic measurements in high pressure reactors with the surface science world. Here, molecular beam techniques establish unique possibilities to study surface kinetics and dynamics in a highly systematic, detailed and quantitative way.[14−18] The advantages of the approach mainly arise from the fact that a kinetic measurement employing molecular beams inherently represents a single scattering experiment, i.e., every molecule interacts only once with the sample surface. Briefly, we may summarize these advantages in comparison with other kinetic probes as follows:

- In an experiment, where there is only a single interaction of the reactant molecule with the surface, we can effectively "count" the surface events, i.e., determine absolute probabilities for different reactive and nonreactive surface events.
- We have the possibility to perform fast and flexible flux modulations, as we do not have to deal with diffusion, viscous flow, or pumping issues. This allows us to perform fast and precise studies of transient processes.
- In contrast to temperature programmed experiments, many molecular beam experiment can be performed under isothermal conditions, simplifying the analysis of the kinetics.
- A large degree of control over the properties of the impinging molecules is provided, such as, e.g., their kinetic energy, the angle of incidence or their internal energy. This enables us to perform studies of the dynamics of the gas−surface interaction.
- Finally, the experiment is performed at low background pressure, which (a) suppresses background reactions and (b) enables us to investigate the dynamic properties of the desorbing/scattered products and reactants, such as their angular distribution and kinetic energy. Besides studying the reaction/desorption potential energy surface (PES), such experiments may potentially be employed to probe site or facet specific kinetics on a heterogeneous surface.

These unique possibilities have motivated a large number of kinetic studies on single crystals (see, e.g., references in ref 14−18). However, similar work on more complex surfaces is extremely scarce and limited to relatively simple beam experiments and very few reaction systems.[19−38] Yet, these studies show already indications for the appearance of unique kinetic effects on such systems.

To systematically perform beam experiments on complex model catalysts, we have designed and set up a new beam apparatus, which is reviewed in section 2.[39] For the first time, it combines up to three beam sources crossed on the sample surface, angle- and time-resolved gas-phase detection, and time-resolved IR reflection absorption spectroscopy (IRAS). The beam experiments are performed on well-defined supported model systems, which are briefly introduced in section 3. Finally, we review a variety of representative experiments from our recent work. Here, we provide examples, which show how to take advantage of most of the unique features of a kinetic beam experiment discussed above. More details about the corresponding experiments can be found in the original literature.[39−47] The considered processes range from adsorption kinetics on supported particle systems and particle size dependent desorption kinetics (section 4) to systematic measurements of transient and steady state rates in conjunction with in-situ surface spectroscopy (section 5). It is illustrated how systematic experiments in this field can help to identify particle size dependencies, which might be easily missed, otherwise (section 6). The origin of such size dependencies is discussed within microkinetic models taking into account the inherent heterogeneity of the model system (section 7). As a possibility to directly access detailed kinetic information on nanostructured surfaces, investigations of the angular distribution of products are presented and are discussed as an experimental probe for site specific reaction rates (section 8). Finally, we summarize recent work and discuss future possibilities of the molecular beam approach, in particular with respect to its applicability to surfaces and reaction systems of increasing complexity (sections 9 and 10).

2. The Molecular Beam Experiment

Motivated by the unique experimental possibilities of the method, combined molecular beam/surface science experiments have been designed and set up in a number of research groups. Most of these experiments have been successfully applied in studies of the kinetics and dynamics of reactions on single-crystal surfaces (see, e.g., refs 14, 16, 17, and 48−55 and references therein). However, similar studies on more complex surfaces are scarce and have been limited to simple single beam setups, so far.[19−38] To expand the scope of experimental possibilities toward the field of model catalysis, a new beam apparatus—specifically designed for kinetic studies at complex surfaces—has been set up at the at the Fritz-Haber-Institute, Berlin.[39] For the first time, the apparatus combines multiple beam sources, time-resolved in situ surface spectroscopy, and angle- and time-resolved gas-phase detection.

The system has been described in detail, recently.[39] Briefly, the model surfaces (see section 3) are prepared in a separate UHV-chamber and subsequently transferred to the scattering chamber, which is schematically displayed in Figure 2. The reactant gases are provided by a chopped/pulsed beam generated from a supersonic expansion and two modulated effusive beam sources based on multichannel arrays. Due to its narrow kinetic energy (KE) distribution and well-defined intensity profile, the first type of beam source is typically used in scattering experiments or sticking coefficient measurements. The second type of source, which easily provides variable beam intensities, is preferentially employed in systematic reaction rate measurements. Total reaction rates are detected via a non line-of-sight quadrupole mass spectrometer (QMS). Additionally, a differentially pumped rotatable QMS is used for angle-resolved reaction rate measurements. Simultaneously, surface IR spectroscopy (IRAS, infrared reflection absorption spectroscopy) under steady state and transient conditions is performed at

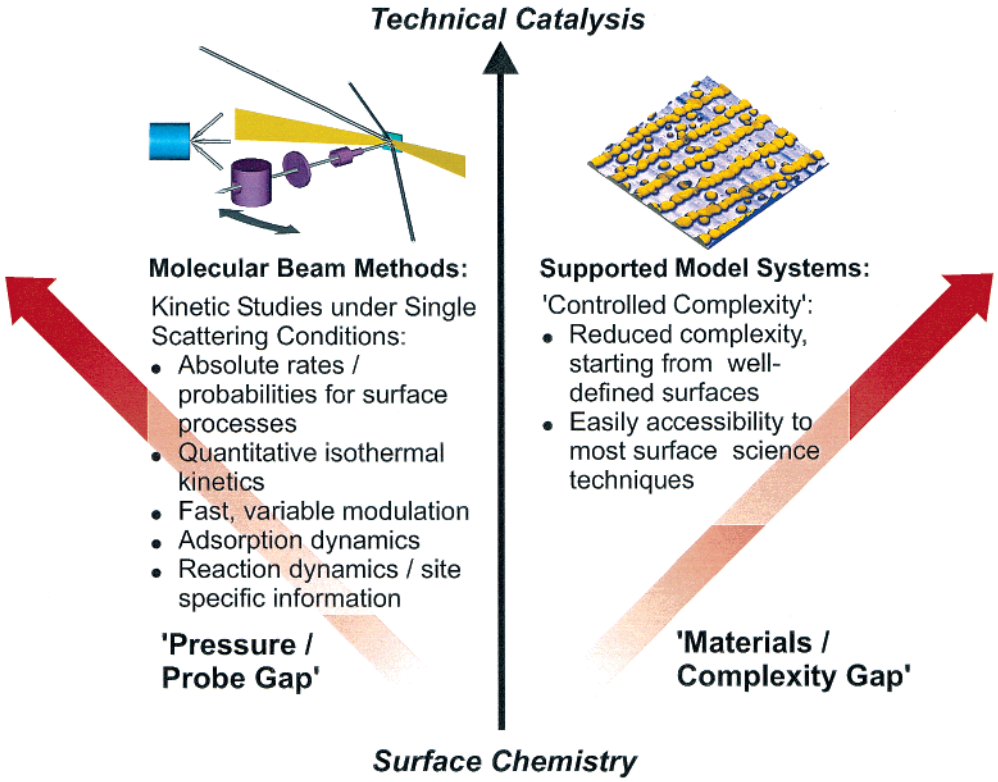

Figure 1. Advantages of a combined molecular beam and model catalyst approach in overcoming the gaps between surface science and catalysis.

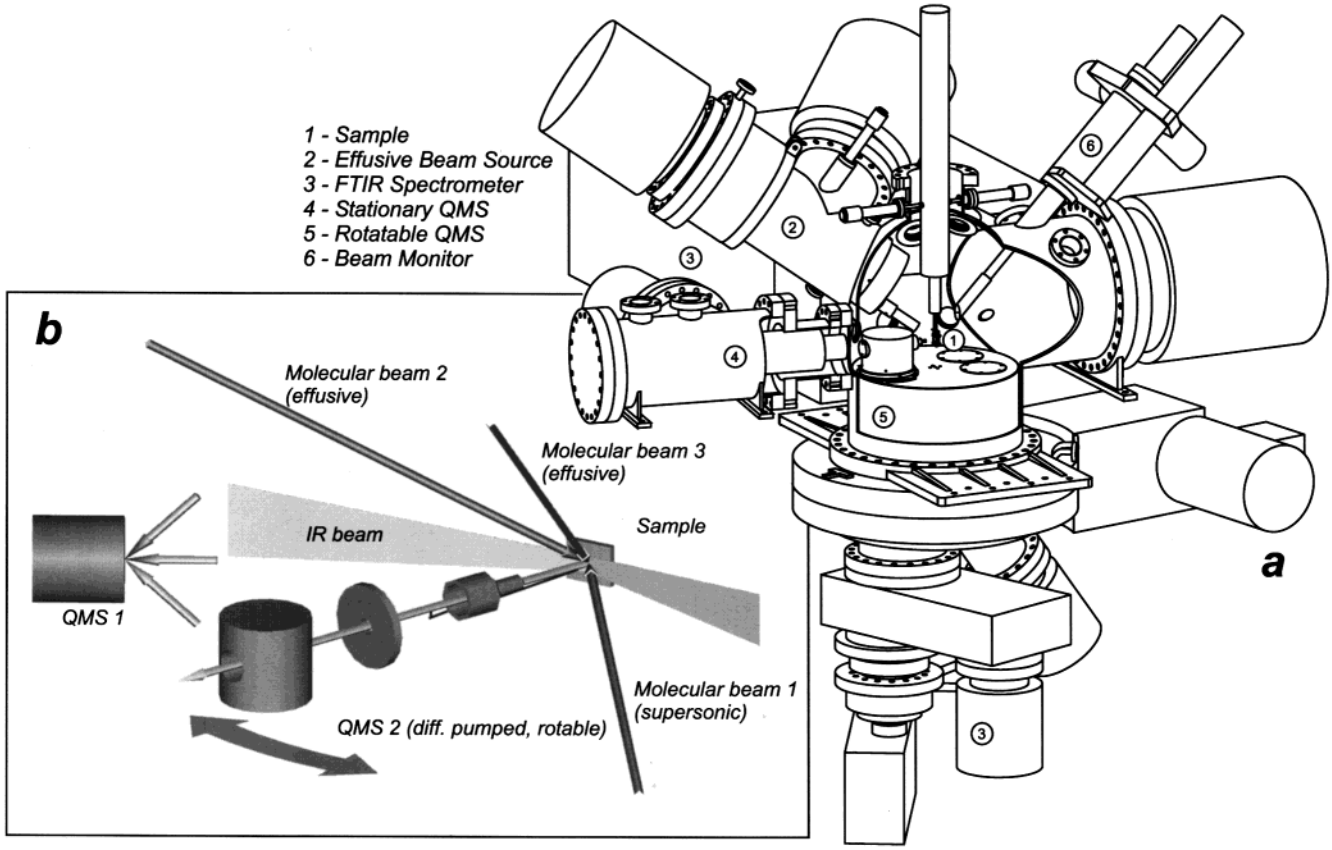

Figure 2. The molecular beam/spectroscopy experiment used in the kinetic studies on complex model catalysts: (a) scattering chamber and (b) schematic representation of the experimental setup.[39]

grazing reflection geometry. Previously, we have demonstrated a temporal resolution of this method up to the ms-regime, which is typically the time-scale on which the surface coverages can be modulated in a beam experiment.[39] For further details on the experimental procedures and a full description of the system we refer to the literature.[39]

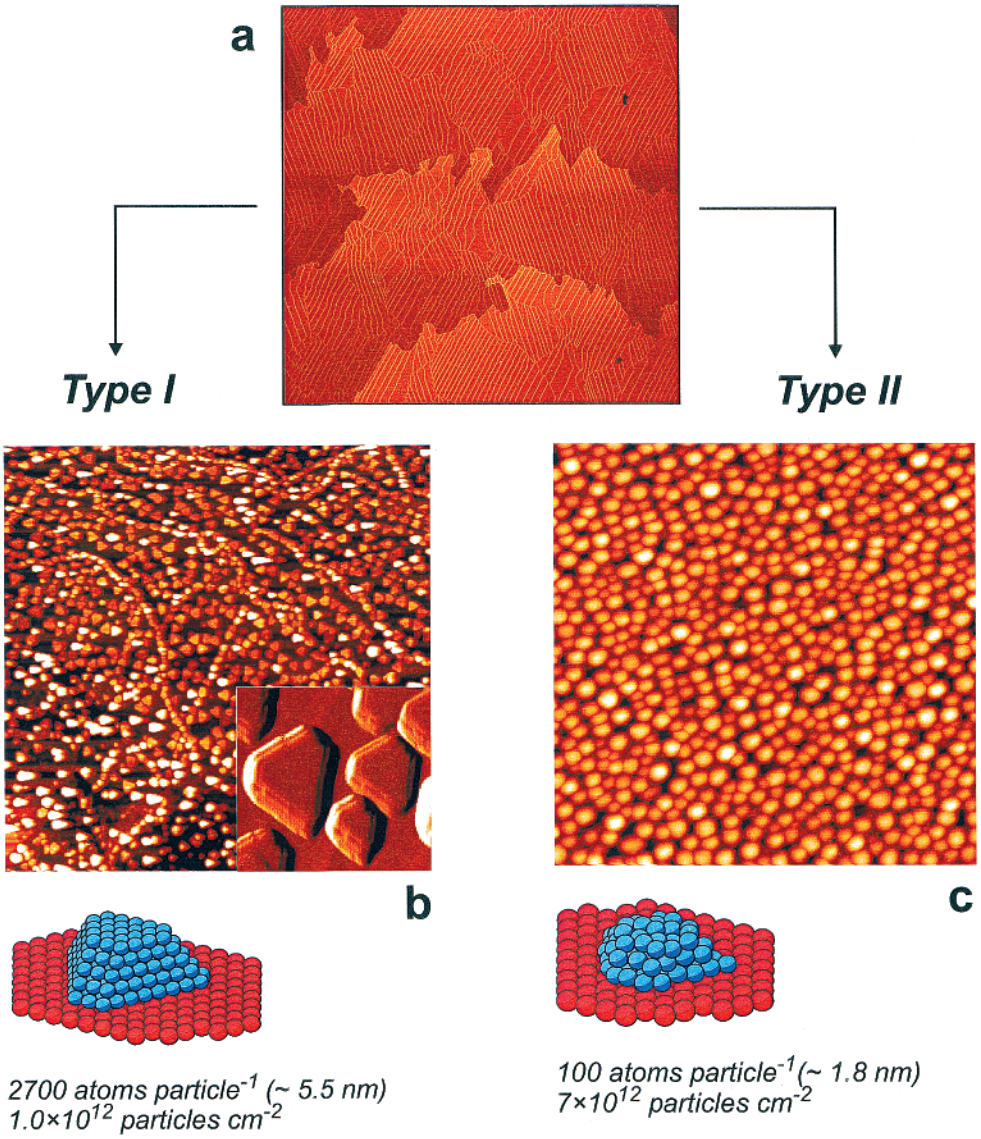

Figure 3. The preparation of well defined supported model catalysts on ordered oxide films: (a) STM image (1000 nm × 1000 nm) of an ordered Al_2O_3 film prepared on a NiAl(110) single crystal, (b) STM image of Pd particles of type I (300 nm × 300 nm) and close-up (20 nm × 20 nm),[41] and (c) STM image of Pd particles of type II (100 nm × 100 nm).[81]

3. Model Systems

Various types of model systems for supported catalysts have been developed during the last years. Their structural characterization, adsorption properties and reactivity have been reviewed, recently.[6,13] In the following experiments, we focus on a particular type of models developed in our group.[7,13] The preparation of these systems is schematically depicted in Figure 3: We start from an alumina film, grown by oxidation of a NiAl(110) single crystal surface. This alumina film is well-ordered, highly reproducible with respect to its preparation and, in our previous work, it has been characterized extensively with respect to its geometric structure, electronic structure and adsorption properties.[10,11] Here, we use the film as a support for metal nanoparticles. In the following, we specifically consider supported palladium particles as a system, which is highly active and relevant for the CO oxidation reaction. The Pd is deposited on the model support by vapor deposition under UHV conditions. Extensive studies have shown, how the properties of the particles such as the particle size, density and structure can be varied over a large range by carefully choosing the appropriate preparation conditions.

In the following, we will focus on two representative types of Pd nanoparticles, which we will denote as type I and type II particles, respectively. The corresponding structural characteristics are summarized in Figure 3. The particles of type I represent relatively large and well-ordered crystallites. These contain an average of approximately 2700 atoms/particle and are mainly terminated by (111)-facets. In contrast to these particles, the Pd aggregates of type II correspond to a small particle size (containing about 100 Pd atoms/particle in average) and are characterized by a defect-rich surface structure (i.e., a higher density of edge, corner, and borderline sites, and a distorted lattice). A more detailed description of the structural properties of these model systems can be found elsewhere.[43]

We will compare the adsorption and desorption kinetics on the two particle types and finally discuss, how the variations in the adsorption/desorption properties can be correlated to differences in reactivity.

4. Adsorption and Desorption Kinetics on Supported Model Catalysts

As the most simple type of experiment we start with a discussion of single beam adsorption and desorption measure-

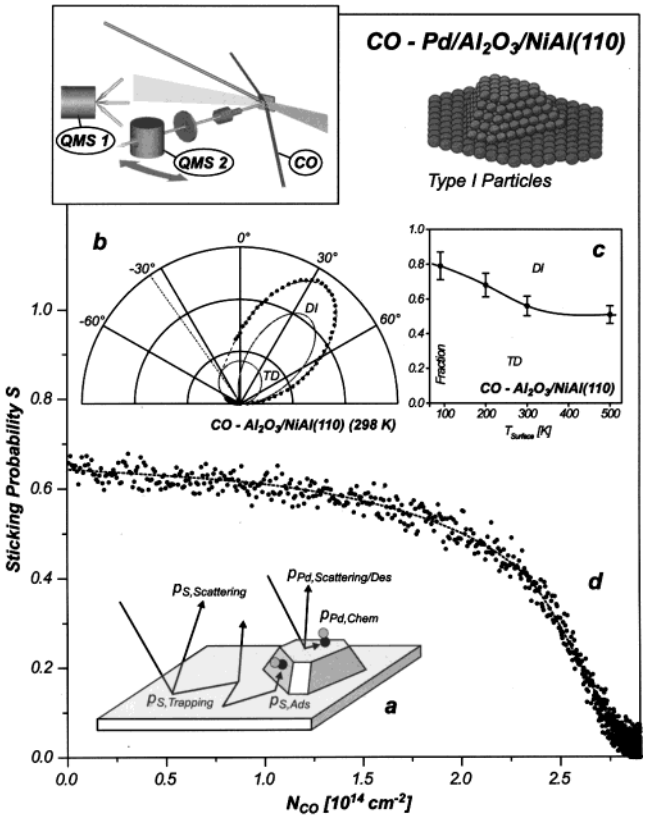

Figure 4. The adsorption kinetics on supported model catalysts: (a) schematic representation of the adsorption and scattering processes, (b) angle-resolved scattering of CO from the ordered Al_2O_3 model support, (c) direct inelastic scattering and trapping desorption contribution for CO scattered from the ordered Al_2O_3 model support, and (d) sticking probability for CO impinging on the Pd/Al_2O_3 model system (type I, 298 K).[40]

ments. The setup is schematically depicted in the inset in Figure 4. We use a beam of CO or O_2 with a well-defined kinetic energy. The beam is generated in a supersonic expansion and impinges on the supported model catalyst at a given angle of incidence. We may now either detect the angular distribution of the scattered/desorbing molecules by angle-resolved mass spectrometry or the total flux of desorbing molecules by angle-integrated mass spectrometry. Additional information on the kinetic energy of the scattered/desorbing molecules and surface residence time of the adsorbates can be derived from the temporal response to a flux modulation of the incident beam (see, e.g., refs 15 and 56).

To start with, we consider an adsorbate molecule, impinging on the oxide support (see Figure 4a). This molecule may either be directly scattered back into the vacuum or it may loose a sufficient amount of kinetic energy during the collision event to be trapped in a physisorbed state on the support. Please note that the adsorbates under consideration here (mainly CO and O_2) adsorb only weakly on the alumina surface. Subsequently, the trapped molecules will diffuse over the support and may eventually desorb. If, however, the diffusing physisorbate encounters a Pd particle within its residence time on the surface, the molecules can chemisorb on the metal surface. As has been discussed in the literature,[19,20,57,58] this so-called "capture zone" or "inverse spillover" effect may substantially enhance the adsorbate flux to the particle and, under certain conditions, will have to be taken into account in a microkinetic modeling.

It is worthwhile to point out that the molecular beam experiment enables us to differentiate between the different adsorption, desorption and scattering channels (Figure 4a). This is possible as the directly scattered molecules can be distinguished from the trapping/desorption channel by both their angular distribution and their kinetic energy. While the molecules directly scattered from a flat surface show a lobular angular distribution which is peaked close to the specular direction and are characterized by a kinetic energy which is related to the energy of the incident beam, the trapped and desorbing molecules have been accommodated to the surface temperature. Consequently, their kinetic energy will depend on the surface temperature and their angular distribution will in general be symmetric with respect to the surface normal.

In Figure 4b a characteristic angular distribution is shown for CO scattered from the clean alumina model substrate. Typically, two contributions can be identified, a lobular contribution from the directly scattered part and a broad symmetric contribution from the trapping/desorption component. Additional evidence for the presence of the two channels can be derived from time-of-flight measurements (not displayed). The relative fractions of the trapping and the scattering component can be quantified and depend on the substrate temperature (see Figure 4c). For a more detailed discussion of this effect we refer to the literature.[40]

The effect of the "capture zone" zone is clearly illustrated in a sticking coefficient measurement, which is displayed in Figure 4d. In this type of experiment we determine the total probability for an impinging molecule to be chemisorbed on the sample surface.[59,60] For the example displayed here, the initial sticking probability corresponds to about 65%, despite fact that for the type I Pd particles only 20% of the total surface is covered by Pd. This demonstrates that the main fraction of the adsorbates is supplied via the "capture zone" and not via direct impingement and adsorption on the particle. Depending on the structural properties of the catalyst and the reaction systems under consideration, the effect can be even more pronounced. In particular at low reaction temperatures the adsorption kinetics may be strongly dominated by the support (see, e.g., ref 33). It is apparent that under conditions under which the adsorption kinetics of a reactant involves some degree of rate control, the support "capture zone" has to be taken into account in a proper microkinetic modeling. With respect to the application of beam techniques, it is most important to point out that by combination of the gas-substrate scattering data, the sticking coefficient measurements and the structural data on the model surface it is possible to determine the probabilities for all elementary steps in the previous discussion, i.e., scattering, trapping, adsorption, support diffusion, and "capturing" (see Figure 4a). Thus, the beam experiments can provide a method to quantify this information as well as to verify and refine kinetic models.

Besides the adsorption process, which was discussed so far, we may also probe the kinetics of desorption processes. This is normally done by employing a modulated beam source and detecting the temporal response by mass spectrometry, either in a angle-resolved or an angle-integrated fashion. A corresponding experiment for CO adsorption/desorption is displayed in Figure 5a. Further details can be found elsewhere.[47] We expose the Pd/alumina model surface to a modulated CO beam generated by a supersonic beam source and detect the integral gas phase response. Once the CO beam is switched on we observe an instantaneous rise in the CO pressure due to the fraction of impinging molecules, which are directly scattered or are trapped and desorb from the support. Similar as in a conventional sticking coefficient experiment,[59,60] we subsequently find a slower rise in the CO signal due to the decreasing

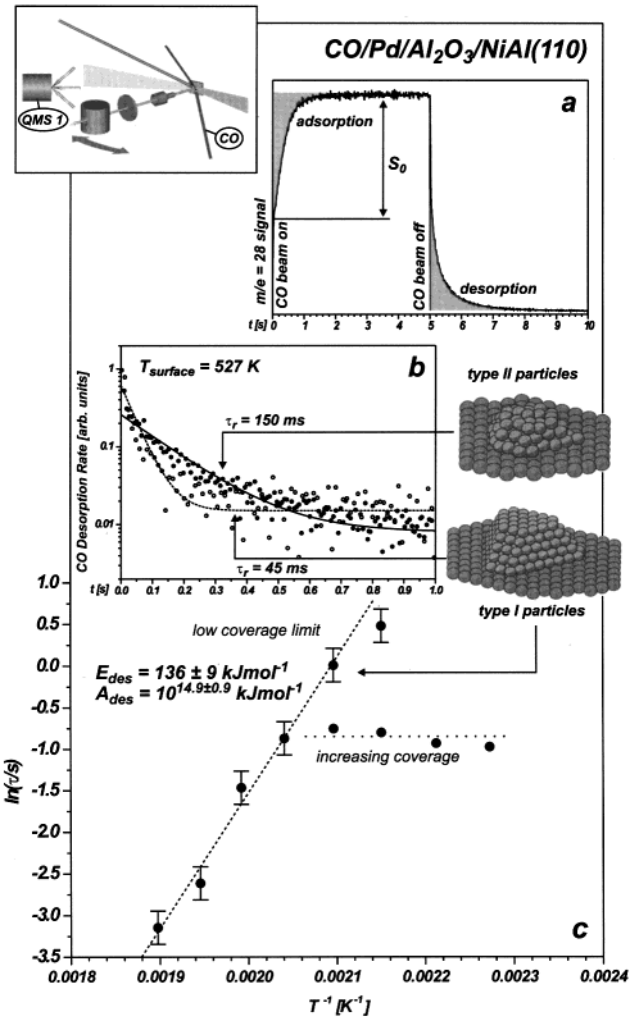

Figure 5. The desorption kinetics from supported Pd model catalysts: (a) a modulated CO beam adsorption/desorption experiment (see text), (b) Comparison of the residence times of CO on Pd particles of type I and type II in the low coverage limit, and (c) Desorption parameters for the large Pd particles of type I as determined from a modulated beam experiment.[47]

net fraction of chemisorbing molecules as we are approaching adsorption/desorption equilibrium. Once the beam is terminated, the process is reversed, i.e., an instantaneous decrease in the CO pressure is followed by a slower decrease due to desorption from the Pd particles. (Note that the residence time on the support is typically $<10^{-9}$ s, i.e., desorption is instantaneous under our experimental conditions. Thus, the desorption rate from the Pd particles is probed, exclusively.) From the rate, the desorption time constant can be determined as indicated in Figure 5b. If the experiment is performed as a function of the surface temperature, the activation parameters for CO desorption from the model surface can be calculated. The corresponding values for the type I Pd particles are given in Figure 5c. As expected for this type of particles, which are largely terminated by (111) facets, the values of the desorption energy and preexponential factor are in good agreement with experimental data for Pd(111) single-crystal surfaces (desorption activation energy: 134 ± 8 kJ mol^{-1}, preexponential factor: $10^{14.4\pm0.8}$ s^{-1} [61,62]). It has to be pointed out that both the supported particle system and the single-crystal values correspond to a low coverage limit ($\theta \leq 0.1$). At higher coverages (i.e., at higher pressures or lower sample temperatures) adsorbate interactions result in deviations from a simple first order desorption kinetics, i.e., the desorption rate constant becomes strongly coverage dependent ("high coverage" residence times in Figure 5c) (see, e.g., ref 47 for more details).

If we now compare the residence times in the low coverage limit and under identical conditions for the two types of Pd particles (Figure 5b), significantly larger values are found for the smaller and defect-rich particles of type II. From the difference in the residence times, an increase in the desorption activation barrier of approximately 5 ± 2 kJ mol^{-1} can be estimated for the smaller particles. This observation is consistent with thermal desorption spectroscopy data, which show an increase in the maximum desorption temperature with decreasing particle size.[47]

There is, however, a second effect which may be extracted from these desorption experiments, which is an increased fraction of CO desorbing in the low-temperature regime, i.e., at temperatures below the main desorption feature.[7,13,47] This observation indicates that besides the more strongly adsorbed states, there are more weak adsorption states available on smaller particles. This result is corroborated by X-ray absorption studies on the same system[13,63] and theoretical investigations of CO adsorption on Pd clusters and stepped surfaces.[64,65]

We can summarize these particle structure dependencies by concluding that with decreasing particle size we observe an increasing coverage dependence of the Pd−CO bond strength. This means that on small and defect rich particles we find both more strongly CO-bonding sites and more weakly CO-bonding sites as compared to larger well-faceted particles, where the coverage dependence of the CO−Pd adsorption energy is less pronounced. In the following sections we will investigate how these differences in the adsorption properties are reflected in the kinetics of chemical reactions performed on these model systems.

Before addressing the reaction kinetics, however, it is worthwhile to mention that similar experiments as shown here for the adsorption of CO can also be performed for the adsorption of O_2. It turns out that oxygen adsorption on these model systems is complicated by a bulk diffusion process, which has been characterized in detail, recently. A complete discussion of this issue is beyond the scope of this paper and we refer to the original literature.[41,47] Briefly, it is found that stable surface kinetics are obtained only after stabilization of the model system by extended oxygen exposure. Thus, all experiments discussed in the following have been performed on stabilized samples, which maintain activity over a period of time well beyond the experiment times applied in this work.

5. Steady State and Transient Reaction Rate Measurements

As a simple model reaction we will consider the CO oxidation, which is among the best studied reactions in surface chemistry. Molecular beam experiments have been performed early on Pd(111)[61,62,66] and on other single-crystal surfaces (see, e.g., refs 67−70). On supported particle systems, however, the amount of similar experimental work is rather limited (see section 1) and many open questions remain with respect to the role of particle size and structure.

To probe reaction kinetics on our supported model catalysts in a quantitative and systematic manner, we combine rate measurements with static and time-resolved IR reflection absorption spectroscopy.

The experiment is schematically illustrated in Figure 6. We superimpose a modulated molecular beam of CO and a continuous beam of O_2 on the sample surface. The transient

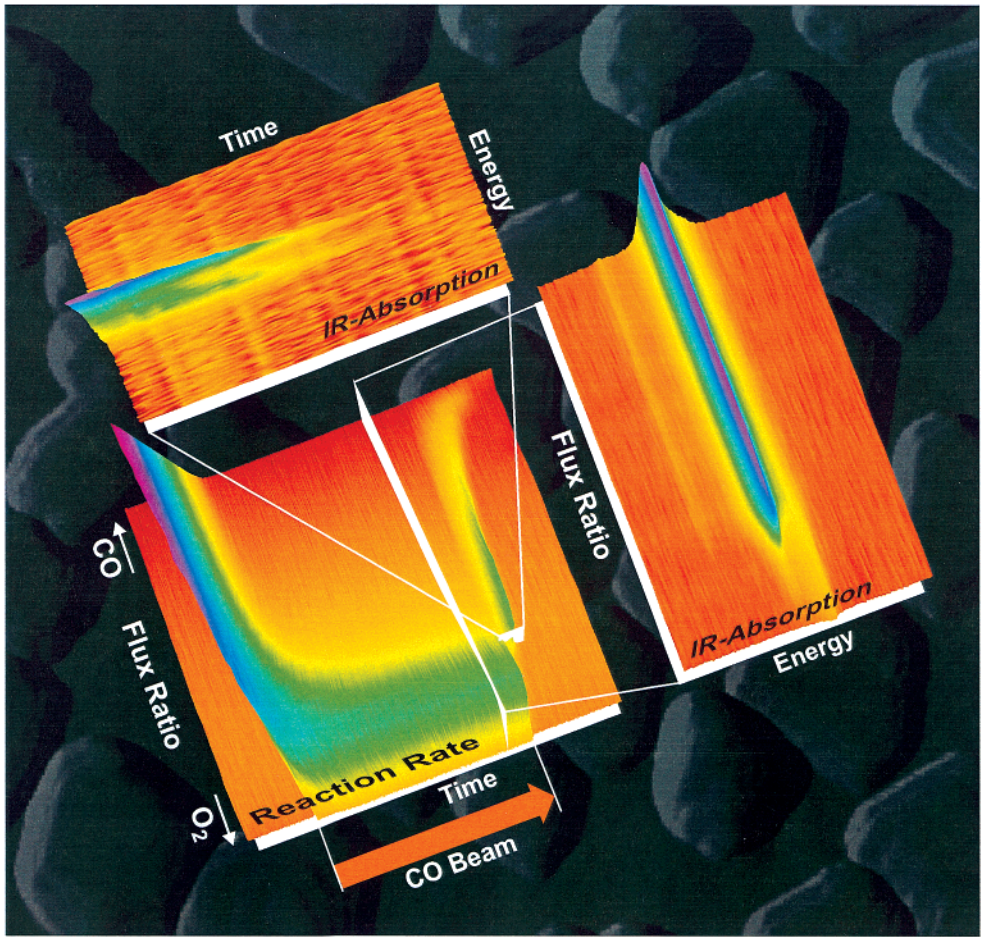

Figure 6. Correlated molecular beam reaction rate measurements and in situ IR reflection absorption spectroscopy on a Pd/alumina supported model catalyst. Bottom panel: Transient reaction rate as a function of the reactant flux ratio. Right part: IR spectra (CO stretching frequency region) under steady-state conditions. Top part: Time-resolved IR spectra under transient conditions. Background: STM image of the supported model catalyst.

CO_2 production rates are recorded (Figure 6, center panel), while the CO beam is switched on for a given time interval (Figure 6, 'time axis' on the center panel). Systematically, the experiment is repeated for different fractions of CO in the total gas flux impinging on the sample, ranging between 0, i.e., pure oxygen (Figure 6, "flux ratio" axis), and 1, i.e., pure CO. In the following, the fraction of CO in the total gas flux impinging on the sample will be denoted as x_{CO}.

Upon switching the CO beam, a transient response in the reaction rate is observed before a steady state is finally established. To obtain information on the adsorbed species under reaction conditions, we perform two types of in situ IRAS experiments: (1) For every flux ratio we record an IR absorption spectrum after steady-state conditions have been established. The corresponding spectra showing the CO stretching frequency region are displayed on the right-hand panel of Figure 6. (2) For any given flux ratio we may also record IR absorption spectra as a function of time after modulation of the CO beam, thus obtaining information on the temporal evolution of adsorbate species and coverages within the transient region. A series of corresponding time-resolved absorption spectra (CO stretching frequency region) are displayed on the top part of Figure 6.

In the following we will consider the different types of experiments in more detail. A typical series of rate measurements is depicted in Figure 7. Note, that in this experiment the CO and O_2 beam intensities can be chosen independently. Typically, we perform a set of measurements such that the CO flux ratio x_{CO} is varied, whereas the total pressure at the sample position is kept constant (10^{-6} mbar for the experiments shown in Figure 7). In this way, we obtain the transient and steady-state reaction rates for all values of x_{CO}.

The steady state reaction rates are plotted in Figure 7c. We can clearly distinguish between two reaction regimes: Under conditions of high oxygen flux we obtain steady state conditions under which the surface is to a large extent covered by oxygen and the CO coverage is low. Here, the reaction rate is proportional to the CO flux (in the following denoted as O-rich reaction conditions). Once a critical CO flux is reached, the surface rapidly switches to the so-called CO-rich steady state. Here, the CO, which accumulates on the surface, inhibits the adsorption of oxygen. As a result of this poisoning effect, the reaction rate decreases rapidly. The described type of behavior as a function of the CO and oxygen flux is well-known from single crystals, and shall not be further discussed here (see, e.g., refs 42, 45. 62, and 66).

At this point, we will concentrate on the transient behavior instead, as it is displayed in Figure 7b. It is apparent that the two reaction regimes, O-rich and CO-rich, are also characterized by a typical transient behavior: (1) Under O-rich conditions (lower trace), we start from an oxygen saturated surface. Upon switching on the CO beam, we observe an immediate rise in the CO_2 formation rate, followed by a slower increase, before, finally, steady-state conditions are reached (see, e.g., ref 31 for a more detailed discussion of the underlying precursor adsorption mechanism). Once the CO is switched off, the remaining

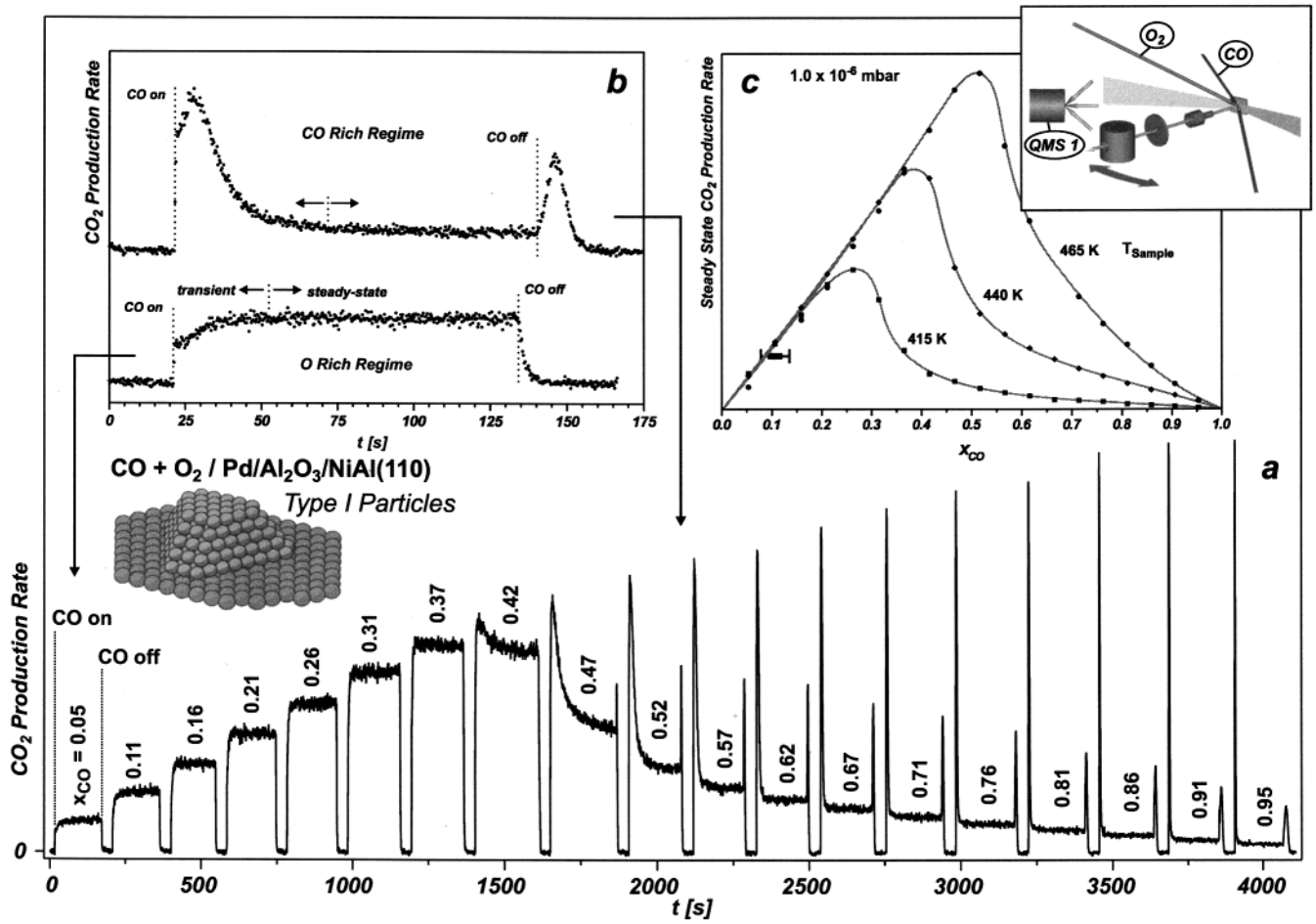

Figure 7. Transient and steady-state CO oxidation kinetics on a Pd/Al_2O_3 model system of type I: (a) transient rates for a continuous oxygen beam and a modulated CO beam as a function of the fraction of CO in the total gas flux, (b) close-up of typical transients under CO-rich and oxygen-rich reaction conditions, and (c) steady-state CO oxidation rates as a function of the CO flux fraction.[42]

low CO coverage will be consumed and the reaction rate drops immediately. (2) Under CO-rich conditions (upper trace), we start again from oxygen saturated Pd particles. Upon exposure to the CO beam, a similar behavior is found, initially. At some point, however, the reaction rate passes through a maximum and drops again. This behavior can be easily understood to be due to accumulation of CO on the surface, which leads to the poisoning effect discussed above. After switching off the CO beam, the process is reversed and again a peak in the CO_2 production rate appears as a result of the decreasing CO poisoning, until finally the reaction rate becomes limited by CO depletion.

Up to this point, the observations can be explained on the basis of simple homogeneous surface models and show no indications for particular effects, which may be specific to supported model systems. However, the situation changes, if we investigate the transient behavior between the two reaction regimes. Here, a peculiar transient behavior is observed (see Figure 8a). It is characterized by a sudden drop in the reaction rates, once the CO flux is terminated, followed by a CO_2 production peak at later time. This effect has previously been observed on other supported Pd model catalyst as well,[19,20] and was related to the presence of defect adsorption states on the Pd particles.[22] Indeed, the desorption experiments discussed in section 4 have demonstrated the presence of different types of adsorption states with modified binding energies, the fraction of which increases with decreasing particle size. Taking this into account, a possible explanation of the modified transient behavior would be a scenario in which upon termination of the beam CO would desorb rapidly from the particle facets and, subsequently, the CO_2 peak would originate from more strongly adsorbed CO at defect sites.[19,20] To probe this hypothesis we have performed time-resolved IRAS experiments within the transient region. The corresponding IR spectra are displayed in Figure 8b together with the total and partial absorption signals (Figure 8c).[42] The most important point with respect to the above discussion is that under no conditions a sudden change in the IR spectra could be detected which was correlated to the drop in the reaction rate. This clearly demonstrated that the transient dip in the reaction rate is not related to a rapid coverage change of a CO majority species. We will come back to this issue and discuss alternative explanations in section 7. Before, however, it is useful to briefly consider the size dependence of this and other effects.

6. Particles Size and Structure Dependencies

To probe the effects of particle size and structure on the transient and steady-state kinetics, we compare sets of experiments under identical conditions for Pd particles of type I and II, respectively. The results are summarized in Figure 9. For both types of particles we find the three reaction regimes discussed in the previous section, i.e., the O-rich and the CO-rich regimes, characterized be their typical transient reaction rate traces and a transition region showing a minimum in the reaction rate after termination of the CO beam (area shaded in gray in Figure 9). We observe, however, a pronounced difference

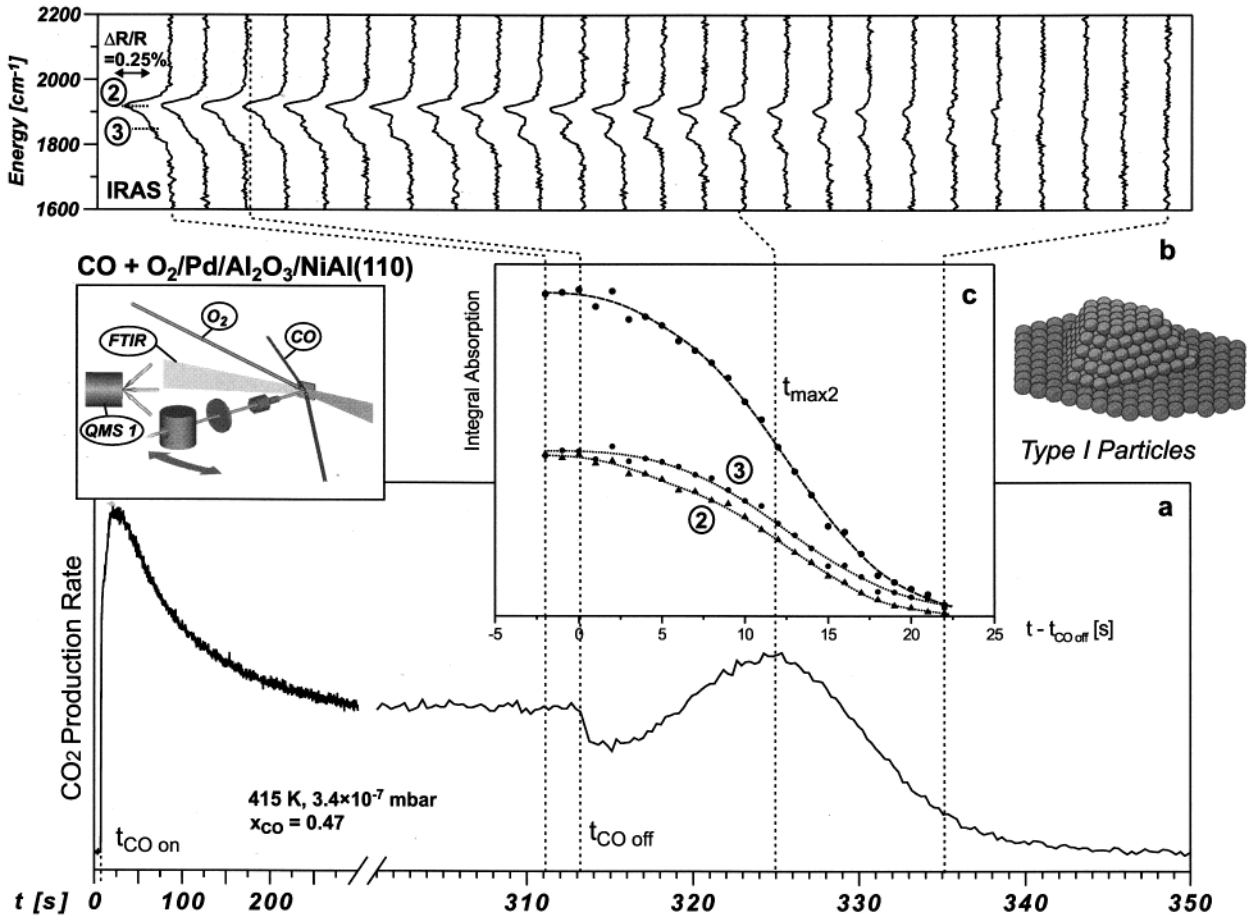

Figure 8. Time-resolved IRAS/transient reactivity experiment for the CO oxidation on a Pd/Al_2O_3 model system of type I: (a) transient reaction rate, (b) time-resolved IR reflection absorption experiment in the transient region, and (c) integral and partial intensities of the CO stretching vibration features.[42]

with respect to the conditions under which the three regions appear. Whereas for the large and ordered particles of type I the transition region is limited to a very narrow range of conditions, for the small and defect rich particles of type II the transition behavior appears over a large range of O_2 and CO fluxes.

A second difference is related to the steady state reaction rates, which are displayed in Figure 9c. As usually done in catalysis, the rates have been normalized to the number of Pd surface sites, which have been calculated from the structural data discussed in section 3. Surprisingly, these normalized reaction rates (turnover frequencies, TOF) show a different particle size dependence for the two reaction regimes: Under oxygen-rich conditions, larger rates are found for the large particles, whereas the reverse dependence is observed under CO-rich conditions. We may speculate that the differences under oxygen-rich conditions may be related to the Pd−oxygen interaction, e.g., to the rate of formation of subsurface oxygen varying as a function of defect density. In the following discussion, however, we focus on the different shapes of the reaction rate curves under CO-rich conditions. Here, the particles of type I reveal a pronounced poisoning effect with increasing CO fraction (Figure 9c, steep drop in the reaction rates for large x_{CO}), whereas the poisoning of the smaller particles is significantly less pronounced (Figure 9c, shallow decrease of the reaction rate for large x_{CO}). In the following, we will attempt to relate these differences to the differences in the CO adsorption behavior discussed in section 4.

Before this, however, we briefly consider, how the reaction rate measurements can be supplemented by in situ IRAS measurements. As a full discussion of the results is beyond the scope of this article, we focus on the most essential features and we again refer to the original publications for more details.[43] Series of in situ IRA spectra of the CO stretching frequency region for the two types of particles are displayed in Figure 10 a and b, respectively. In the spectra, we can clearly differentiate between three distinct absorption regions, which can be attributed to (1) linearly adsorbed CO at (111) facets and defect sites, (2) CO in bridge and hollow sites CO on (111) facets and (100) facets together with CO at defect sites, and (3) CO in hollow sites on (111) facets (see, e.g., refs 13, 71, and 72 and references therein). The total absorption, the relative integral absorption and the stretching frequencies are plotted in Figure 10c to e as a function of the fraction of CO in the reactant flux.

Briefly, the total absorption signals reflect the increasing CO coverage with increasing CO flux under steady-state conditions. However, we have to keep in mind that in surface IR spectroscopy there is no simple relationship between the integral absorption signal and the surface coverage (see, e.g., ref 73). In particular at high coverages, the signal intensities may only weakly depend on the adsorbate densities. Still, certain features can be directly identified from Figure 10, such as the sudden CO poisoning transition for the large particles as a function of x_{CO}. Moreover, we can derive information on the formation of different adsorbate structures depending on the reaction conditions from the relative intensities of the peaks. For the large type I particles (open symbols) strong rearrangements are observed as a function of the CO fraction in the reactant flux. Such coverage dependent rearrangements are characteristic for CO adsorption on Pd(111), a system for which a large number

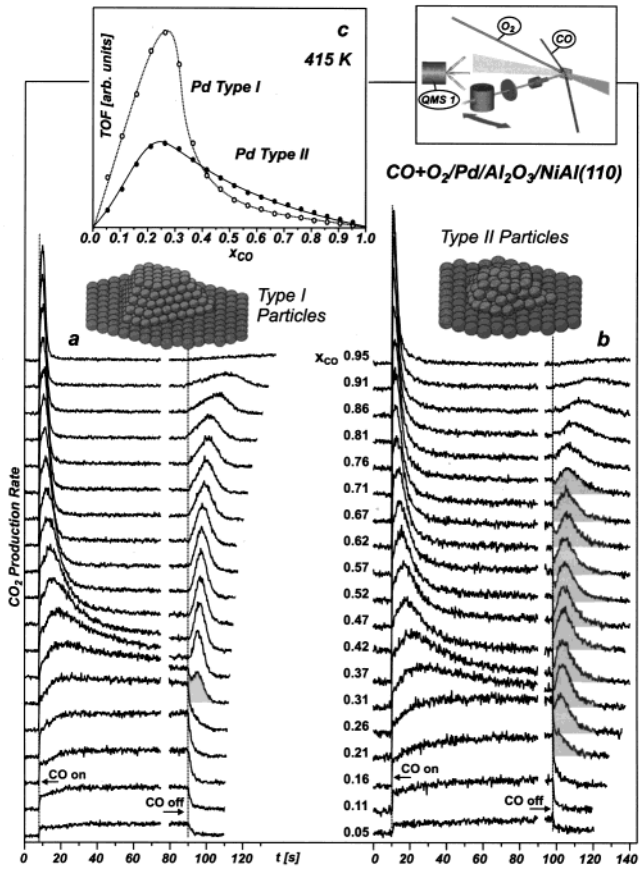

Figure 9. Particle size dependence of the steady state and transient reaction rates on the Pd/Al_2O_3 model systems: (a) transient behavior for the CO oxidation on type I Pd particles (415 K, effective pressure: 10^{-6} Pa) and (b) for the type II Pd particles. (c) Comparison of the steady-state rates for both types of model systems.[43]

of superstructures is found as a function of coverage (see ref 74 and references therein). No similar intensity changes are found for particles of type II. This may indicate that similar structural transitions in the adsorbate layer are suppressed in this case, possibly by the larger differences in adsorption energy (see section 4).

Finally, we investigate the dependence of the CO stretching frequencies on the fraction of CO in the reactant flux (Figure 10e). The frequency shifts are induced by chemical effects (i.e., neighboring CO molecules) or dynamic coupling effects between the dynamic dipoles (see, e.g., ref 73) and may serve as an indicator for the local adsorbate density. Again, we can clearly identify the sudden increase in the CO density related to the transition between the two reaction regimes.

7. Microkinetic Models and Discussion

In the previous sections we have shown how we can identify specific kinetic effects on supported model systems and particle size dependencies by performing systematic beam experiments under both steady state and transient conditions. These effects have also been investigated by static and time-resolved in situ IR spectroscopy.

In this section we will briefly touch the question how such effects can be understood on a microscopic level and corresponding microkinetic models can be developed. To begin with, we will reconsider the transient measurements displayed in Figure 7. Recently, we have simulated this type of experiment on the basis of a mean-field model of a homogeneous surface[42] and the kinetic parameters for Pd(111).[61,62] It is found that the general kinetics on the large particles of type I is well described by this model. However, deviations remain in the transition region between the O-rich and the CO-rich reaction regime. In particular, the homogeneous surface model fails to provide a satisfactory description of the transient reaction rates in this region.

Apparently, certain features of the model system cannot be fully described by the simplified homogeneous surface model. Naturally, we might anticipate that these features are related to the heterogeneity of the model catalyst surface, as schematically illustrated in Figure 11. The supported model catalyst consists of a large number of active metal particles. Depending on the reaction conditions, these particles will behave like by more or less isolated microscopic reactors. On every particle we find various types of reactive sites: Apart from regular sites on the dominating type of crystallite facets (in our case (111) facets for the Pd particles of type I), a different type of minority facets may coexist (e.g., (100) facets). The microfacets are separated by edge and corner sites. Moreover, steps may be present on the particles and interface sites are exposed at the particle perimeter. The differences in the electronic and geometric structure between these different types of sites will result in locally varying adsorption, desorption, and reaction rates.

With respect to the overall kinetics, it turns out to be an important question, whether surface diffusion facilitates an exchange of adsorbates between these different types of adsorption sites (see, e.g., ref 75). Here, we may differentiate between two limiting cases: In the first scenario, we anticipate that the different sites are located on a single particle. This case we will denote as *intraparticle* heterogeneity. If surface diffusion of the adsorbed species is rapid under reaction conditions, thermodynamic equilibrium is established between the coverages on the different particle areas. In the particular case of CO oxidation, we anticipate that CO diffusion is fast on the time scale of the surface reaction (ref 76 and references therein). On the other hand, little is known experimentally on the diffusion rates of oxygen under similar conditions. Possible experimental strategies addressing this open question will be discussed in section 8.

In the second limiting case we assume coexisting particles, which are characterized by different mean adsorption, reaction, or desorption rates. Such deviations could, for example, arise as a consequence of different particle sizes or as a consequence of a different degree of ordering. Additionally, we might have to take into account differences in the particle surrounding, which, as a consequence of the "capture zone" effect discussed in section 4, can result in different adsorption rates. This type of structural complexity we will denote as *interparticle* heterogeneity. Here, the exchange of adsorbates between the different particles via surface diffusion will strongly depend on the adsorption properties of the support, the particle distance and the reaction conditions. For sufficiently weakly interacting supports, surface diffusion will be strongly suppressed and the particles will behave like largely isolated systems.

For the *interparticle* heterogeneity case, the specific transient behavior in the transition region between the O-rich to the CO-rich regime (sections 5 and 6) can be easily rationalized in the following way: Close to the transition region between the O-rich and the CO-rich reaction regime, we anticipate that due to local variations of the adsorption, desorption and reaction rates, a fraction of the particles switch to a CO-rich state, whereas other particles remain in an O-rich steady state. In this case, the total reaction rate is a superposition of both types of transients, with their relative contribution depending on the given set of reaction

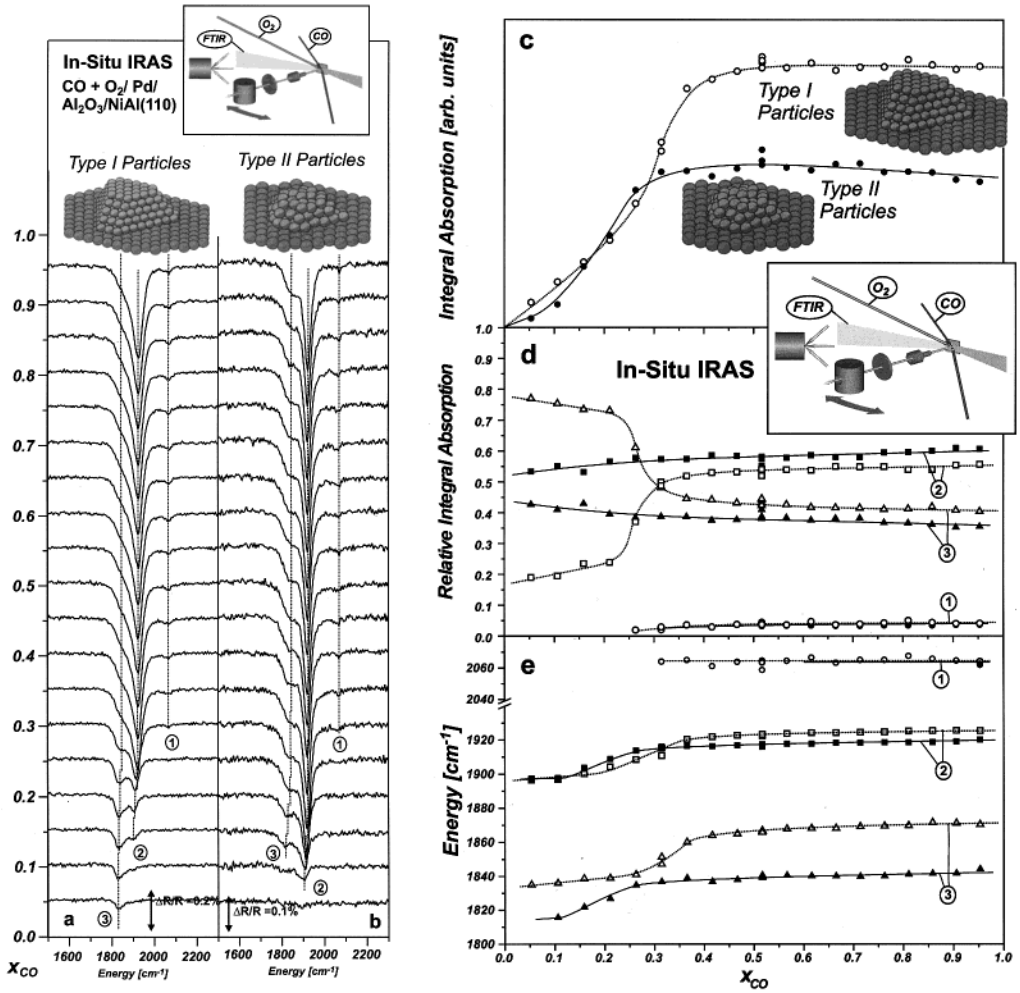

Figure 10. In situ IR reflection absorption spectra recorded under steady-state conditions: (a) CO stretching frequency region for Pd particles of type I (415 K, effective pressure: 10^{-6} Pa), (b) CO stretching frequency region for Pd particles of type II; (c) Integral absorption for both types of particles, (d) relative intensities of the CO features indicated in (a) and (b), and (e) Stretching frequencies of the CO features indicated in (a) and (b) (open symbols, type I particles; solid symbols, type II particles).[43]

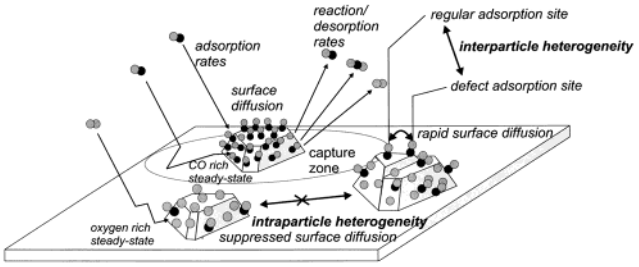

Figure 11. Schematic representation of the different types of heterogeneity on a supported model catalyst and their relation to the reaction kinetics.

conditions. This scenario qualitatively explains the experimentally observed behavior.

To investigate this idea in more detail, we have compared simulations of the transient experiments on the basis of improved mean field models, the key issues of which are summarized as follows (see ref 45 for a detailed discussion): Briefly, we consider a surface, which consists of a majority of regular sites and additionally introduce a minority of defect sites. At this point we use the results discussed in section 4, where both more strongly and more weakly adsorbed CO species were found on the smaller particles. The time-resolved IRAS experiments described in section 5, on the other hand, have revealed that the more strongly adsorbed CO species cannot represent the key species, which is responsible for the modified transient behavior. Thus, we specifically consider the influence of a more weakly adsorbed defect species. In the model we may either assume rapid surface diffusion of CO equilibrating the corresponding coverages (interparticle heterogeneity model) or we can neglect surface diffusion (intraparticle heterogeneity model). Typical simulated transients and the steady-state rates for both cases are displayed in Figure 12.

It is immediately apparent that the characteristic transition behavior, i.e., the pronounced dip in the reaction rates, is reproduced by both types of models (see Figure 12b,c). Moreover, an analysis of the steady state rates exhibits a strongly reduced CO poisoning at high CO flux, similar as experimentally observed for the smaller particles of type II (Figure 12a). The latter trend can be rationalized by taking into account that the weaker adsorption sites are less prone to CO poisoning and thus open a channel for oxygen adsorption, even under conditions under which the homogeneous single crystal surface would already be fully poisoned by CO.

Finally, we would like to conclude at this point that all kinetic effects observed for the small and defect rich particles of type II are well reproduced by the heterogeneous surface model. Despite the qualitative nature of the present model, this example illustrates that it possible to understand particles size effects on complex model surfaces by explicitly accounting for the complexity of the surface in appropriate microkinetic models.

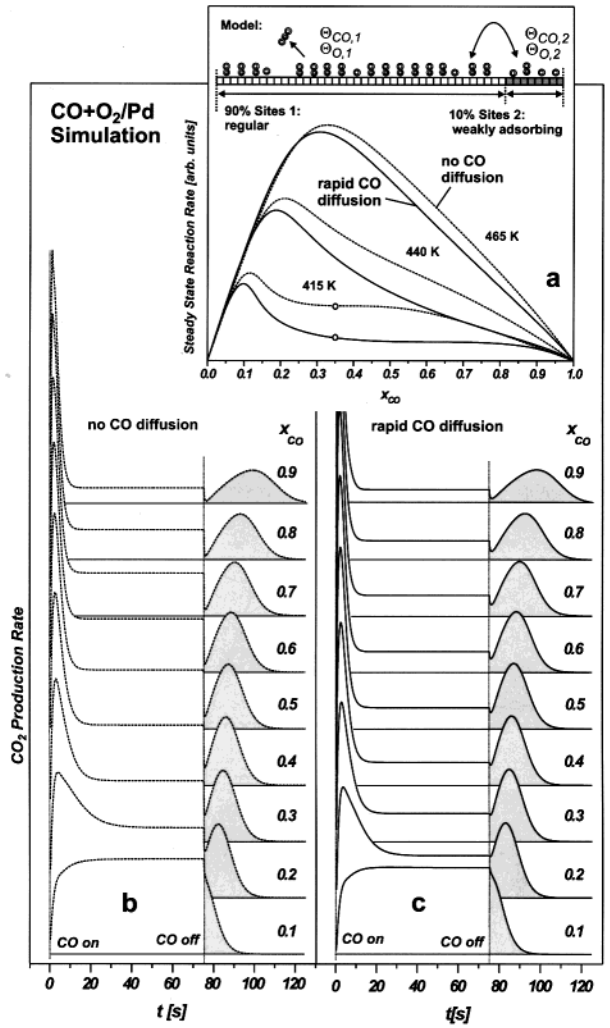

Figure 12. Simulation of the transient and steady-state reaction rates on the basis of a heterogeneous surface model (effective pressure: 10^{-6} Pa): (a) steady-state reaction rates, (b) transient reaction rates neglecting, and (c) including surface diffusion (see text, 10^{-6} Pa, 415 K).[45]

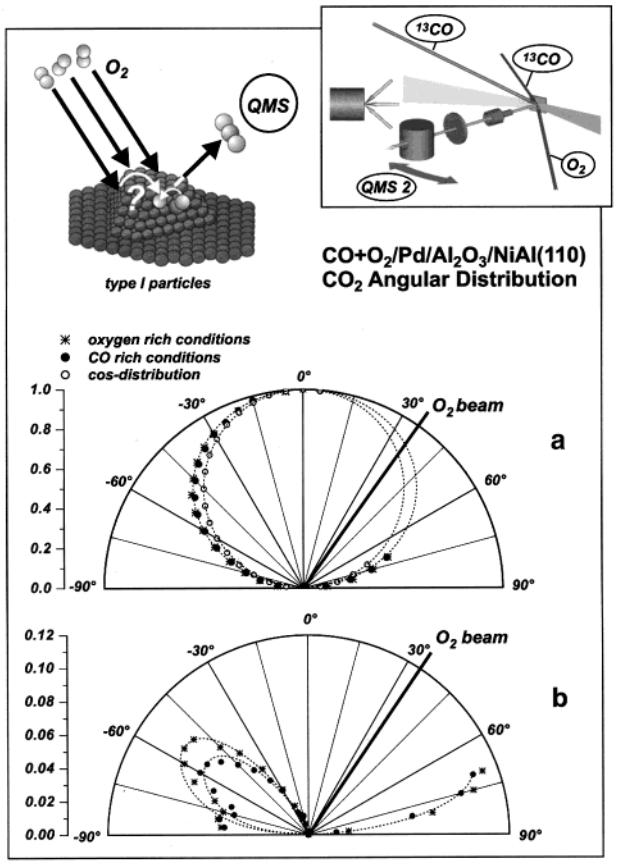

Figure 13. Angular distribution of CO_2 desorbing under steady-state conditions from a type I Pd/Al_2O_3 model system: (a) angular distributions of CO_2 under CO- and O-rich reaction conditions. For comparison a cosine distribution (open circles) is displayed. (b) Difference of the observed angular CO_2 distributions and a cosine distribution.[46]

8. Angle-Resolved Reaction Rate Measurements

In the previous sections we have discussed the role of different reaction sites on a complex catalyst surface and the possible coupling between the sites via surface diffusion. Unfortunately, there are hardly any experimental methods, which allow measurements of site specific reaction rates. Potentially, fast scanning microscopy (see, e.g., refs 77 and 78) or photoelectron microscopy (see, e.g., ref 79) may provide such information; however, these methods remain limited with respect to the accessible range of experimental conditions and the kinetic information supplied.

In the following we will briefly outline, how such information could be possibly derived from a molecular beam experiment. We will take advantage of the fact that in the case of CO oxidation adsorption of CO_2 is extremely weak and thus desorption occurs on a very short time scale after formation of the product molecule (see, e.g., ref 66). The angular distribution of the desorbing molecules will be determined by the potential energy surface (PES) governed by the immediate surrounding of the adsorbate. For the CO oxidation on Pd(111) at low coverage the angular distribution of CO_2 has been found to be close to a cosine distribution.[62] At higher coverage, lateral interactions may modify the PES such that the angular distribution of the CO_2 formed becomes highly directed along the surface normal.[80] In any case, we may anticipate that via measurements of the angular distribution of products it should in principle be possible to differentiate between different sites at which the CO_2 is formed. As the most simple example we may consider the top and various side facets of an ordered crystallite such as the Pd particles of type I (see section 3). Reaction on the different facets should give rise to distinctly different angular CO_2 distributions, peaked along the surface normals of the respective microfacets.

We will use this assumption in an experiment schematically displayed in the insets in Figure 13: First we apply a symmetric flux of CO to the sample by superimposing two effusive CO beams (isotopically marked ^{13}CO is used to reduce the background level). These beams are crossed with a third O_2 beam, the incidence angle of which is chosen such that the top facets of the Pd particles and the side facets facing the beam are exposed to similar direct fluxes of oxygen. The side facets on the opposing particle side, however, are shaded from any direct flux of O_2. The angular distribution of desorbing CO_2, as detected by differentially pumped mass spectrometry, may now provide information on the relative reaction rates on the particle facets and in particular on the relative rates on the exposed and shaded side facets. More details on the setup are given elsewhere.[46]

The results of the experiment are displayed in Figure 13a,b for oxidation under CO-rich and O-rich conditions. In both cases, the angular distributions are found to be similar, but broader than a cosine distribution (for comparison, also displayed in Figure 13a). For clarity, the differences to the cosine distribution,

the broadest product distribution on the single-crystal surface, are displayed in Figure 13b. The observation of the sub-cosine angular distribution indicates CO_2 formation and desorption from the side facets of the particles. This suggests that this type of experiment should indeed enable us to directly monitor reaction rates on the various facets of a nanocrystalline system.

As a second observation, it should be pointed out that under all reaction conditions probed, the asymmetry of the angular distribution was below the detection limit of the experiment. In practice this means that although impinging only on one side of the particles, the oxygen is distributed homogeneously over the Pd crystallites on the time scale of the surface reaction. There are several effects which may contribute to oxygen adsorption on the shaded facets among which are, e.g., diffuse scattering of O_2 and diffusion of physisorbed and chemisorbed O_2 precursors. It is reasonable to assume, however, that a complete equilibration of the surface coverages will require rapid diffusion of chemisorbed oxygen, i.e., diffusion which is fast compared to the residence time of adsorbed oxygen, which itself is determined by the surface reaction rate.

To illustrate and quantify this point, we have simulated the steady-state angle-resolved experiments on the basis of a Monte Carlo (MC) algorithm.[46] As a first step in such a type of simulation, we have to build a realistic model of the supported Pd particles. This is done by analysis of the particle morphology as investigated by STM[13,41,47] and construction of a representative "model particle". In a second step, the microscopic MC model (e.g., the number of allowed CO and O neighbors for the various processes and the adsorbate−adsorbate interaction energies) is adjusted such that the experimentally observed steady-state reaction rates and surface coverages are well reproduced as a function of the reactant fluxes and reaction temperatures (see ref 46). Once the steady state reaction rates are reproduced, we can individually vary the adsorption rates on different nanofacets and investigate the influence of oxygen diffusion on the facet specific reaction rates. Finally, a comparison of the experimental results and the simulations enables us derive an estimate of an upper limit for the oxygen diffusion barrier under steady-state reaction conditions.[46]

With respect to future applications it should be pointed out that this type of MC simulation provides a simple way to introduce microscopic complexity into a truly microkinetic model. Thus, they may potentially provide a variety of new insights into the kinetics on complex surfaces as soon as the corresponding kinetic experiments are capable of supplying sufficiently detailed and quantitative data.

9. Conclusions

In this review, we have shown how molecular beam methods can be utilized to study the kinetics of surface reactions on supported model catalysts in a detailed and systematic manner.

The advantages of the molecular beam approach essentially arise from the single scattering conditions of the experiment, in which the reactant molecules encounter only a single interaction with the surface, thus allowing fast and detailed dynamic and kinetic studies.

In a newly developed experiment, we combine multiple beam sources and time-resolved gas phase and surface spectroscopy. We apply the experimental approach to well defined supported model catalysts, based on ordered oxide films. Specifically, we consider Pd particles of different size and structure, which are prepared under UHV conditions on an ordered alumina film. Previously, these systems have been characterized in detail with respect to their electronic and geometric structure and their adsorption behavior. Here we correlate these properties with the kinetics of adsorption and reaction processes.

Starting with the investigation of the adsorption and desorption kinetics of simple adsorbates on the model catalysts, we show how we can identify and quantify the role of the support in the adsorption kinetics. With respect to the adsorption of CO, we discuss the dependence of the desorption kinetics on the particle size and structure. These particle size dependencies are in a second step related to the particle size dependencies observed in the CO oxidation kinetics.

To probe the reaction kinetics, systematic steady state and transient experiments are performed by superimposing two reactant beams of variable intensity on the sample surface. The rate measurements are combined with in situ time-resolved IR reflection absorption spectroscopy. Via this combination of techniques, it is possible to identify differences in the transient and steady state reaction rates as a function of particle size. To pinpoint the origin of these particle size effects, we discuss microkinetic simulations of the experiments, which explicitly account for the heterogeneity of the model surface. It is shown that the effects found under transient and steady state conditions can be fully reproduced by introducing different types of adsorption sites as suggested by the desorption studies.

Finally, we discuss the possibility to obtain site specific information on the reaction rates via measurements of the angular distribution of products. The concept is applied to the adsorbate diffusion during CO oxidation on ordered Pd nanoparticles. The results are compared to Monte Carlo simulations and suggest that oxygen diffusion is rapid on the time scale of the surface reaction.

10. Future Trends and Possibilities

Can we understand reaction kinetics on complex surfaces such as supported catalysts on a microscopic level? The strategy toward this challenging goal, which has motivated our work and that of several other groups (see, e.g., refs 6 and 13 and references therein), is schematically illustrated in Figure 14.

Traditionally, surface science is capable of providing detailed information on simple surface reactions occurring on simple surfaces. The complexity gap which makes the kinetics on realistic catalysts different from such simple systems is 2-fold: First, there is the aspect of *structural complexity*, which has been discussed in detail in this paper. Typically, a realistic catalyst surface is a structurally and compositionally complex and multifunctional interface, exposing various different adsorption and reactions sites. This structural diversity gives rise to kinetic effects, which are inherent to the complex surface and thus cannot be reproduced in single-crystal model studies. To study such effects, we have developed model systems, which allow us to introduce certain features of the real catalyst in a well-controlled fashion. As a first step toward this aim, we have employed supported model catalysts based on ordered oxide films. Whereas relative to the single crystals surfaces these systems are already highly complex, in comparison to the surfaces of real catalysts a large number of features are still missing. To probe the role of these missing features, we are developing improved models including additional aspects, such as, e.g., modified supports or multiple active component systems. In the last years, the rapid development of well-defined model surfaces has been made possible, e.g., by the routine use of microscopic methods under variable conditions, which complement the traditional techniques by providing a microscopic understanding of the local properties of these surfaces.

In addition to the structural aspect, there is, however, a second aspect contributing to the gap between surface science reaction

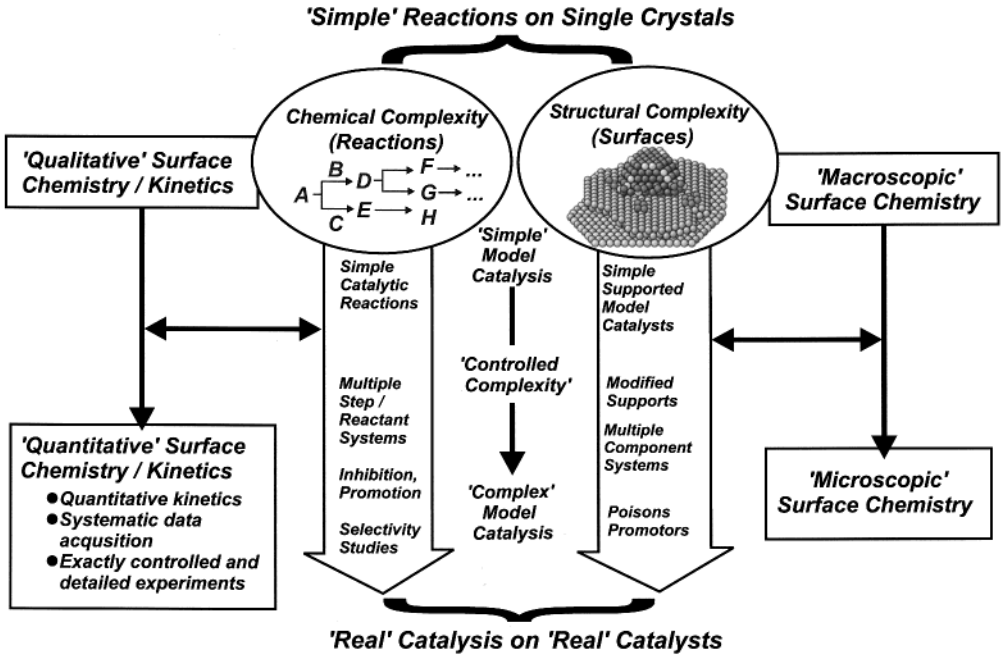

Figure 14. The two sides of the complexity gap between surface science and catalysis.

studies and catalysis. This aspect is related to the types of reaction systems studied in both fields and may be denoted as *chemical complexity*: In many catalytic processes, we are dealing with reaction systems involving multicomponent reactant mixtures as well as multiple steps and pathways. As a consequence, questions regarding intricate poisoning or promotion effects or selectivity issues become most relevant and, at the same time, microkinetic descriptions become highly involved. Most model studies, on the other hand, have focused on relatively simple surface processes so far, among which the most common ones are reactions such as the CO or the NO oxidation. This is particularly true for kinetic studies on more complicated model surfaces such as supported model catalysts (see, e.g., ref 6).

The reasons for this lack of knowledge are closely related to the experimental techniques, which are commonly employed to address surface kinetics in this field. Traditional methods which rely on temperature dependent spectroscopy, desorption or reaction approaches are highly useful in order to obtain qualitative ideas on reaction mechanisms and the underlying energetics. If we would like to address questions such as particle size and support effects or selectivity issues, however, we are typically dealing with relatively small adsorption and/or activation energy differences, which in addition sensitively depend on the reaction conditions. In practice this means that the traditional qualitative experimental methods will not be sufficient in this case. In fact, efforts are inevitable to establish *quantitative* and *systematic* experiment in surface kinetics.

Here, the molecular beam reactor approach, which is situated at the frontier between classical surface science and catalytic reactor studies, provides a number of unique possibilities:

- Experiments yield *quantitative data* under well defined and isothermal conditions.
- Kinetic data can be obtained in a *systematic* way, varying the reaction conditions and reactant coverages. These experiments can be easily *automated* in order to obtain larger databases and improve the reproducibility.
- *Detailed* kinetic information is accessible, taking advantage of the single scattering characteristics of the experiment, which allows fast modulation techniques and access to dynamic properties of reactants and products.

As soon as these experimental possibilities are available, new types of more complex surface processes become accessible. As a step toward this direction, our current and projected work focuses on systems such as the methanol oxidation and partial oxidation (a multistep/multipathway process) or the kinetics of NO reduction under realistic environments (a multiple reactant system).

With respect to these developments toward more realistic surfaces and reaction systems, we expect that the underlying kinetics will also become increasingly complex and in most cases may not be understood intuitively. Thus, in combination with experiments, *microkinetic simulations*, backed up by theoretical calculations, will play a role of strongly increasing importance in this field. Guided by microscopic information on the structural properties and spectroscopic information on the mechanism, the interplay between experiment and modeling may finally lead to an improved microscopic understanding of the reactions kinetics on complex and realistic surfaces.

Acknowledgment. This work has been funded by the Max-Planck-Society and the Deutsche Forschungsgemeinschaft. The authors express their thanks to the co-workers involved in this project, namely Ingo Meusel, Jens Hoffmann, Swetlana Schauermann, Jens Hartmann, and Otto Frank. Moreover, we acknowledge a number of successful collaborations with the groups of G. Scoles (Princeton, NJ), C. R. Henry (Marseille, France), N. Rösch/K. Neyman (Munich, Germany), V. Zdhanov (Novosibirsk, Russia)/B. Kasemo (Göteborg, Sweden), G. Rupprechter and H. Kuhlenbeck (FHI, Berlin, Germany), and finally, M. Bäumer and M. Frank (FHI, Berlin, Germany) for allowing the use of the STM images of the model surfaces.

References and Notes

(1) Ertl, G.; Knoezinger, H.; Weitkamp, J. *Handbook of Heterogeneous Catalysis*; VCH: Weinheim, 1997.
(2) Goodman, D. W. *Surf. Rev. Lett.* **1995**, *2*, 9.
(3) Freund, H.-J.; Bäumer, M.; Kuhlenbeck, H. *Adv. Catal.* **2000**, *45*, 333.

(4) Goodman, D. W. *Chem. Rev.* **1995**, *95*, 523.
(5) Gunter, P. L. J.; Niemantsverdriet, J. W.; Somorjai, G. A. *Catal. Rev.−Sci. Eng.* **1997**, *39*, 77.
(6) Henry, C. R. *Surf. Sci. Rep.* **1998**, *31*, 231.
(7) Bäumer, M.; Libuda, J.; Freund, H.-J. In *Chemisorption and Reactivity on Supported Clusters and Thin Films*; Lambert, M., Pacchioni, G., Eds.; Kluwer Acad. Press: 1997; p 61.
(8) Freund, H.-J. *Angew. Chem., Int. Ed. Engl.* **1997**, *36*, 452.
(9) Rainer, D. R.; Goodman, D. W. *J. Mol. Catal. A* **1998**, *131*, 259.
(10) Jaeger, R. M.; Kuhlenbeck, H.; Freund, H.-J.; Wuttig, M.; Hoffmann, W.; Franchy, R.; Ibach, H. *Surf. Sci.* **1991**, *259*, 235.
(11) Libuda, J.; Winkelmann, F.; Bäumer, M.; Freund, H.-J.; Bertrams, T.; Neddermeyer, H.; Müller, K. *Surf. Sci.* **1994**, *318*, 61.
(12) Bäumer, M.; Libuda, J.; Sandell, A.; Freund, H.-J.; Graw, G.; Bertrams, T.; Neddermeyer, H. *Ber. Bunsen-Ges. Phys. Chem.* **1995**, *99*, 1381.
(13) Bäumer, M.; Freund, H.-J. *Prog. Surf. Sci.* **1999**, *61*, 127.
(14) Rettner, C. T.; Auerbach, D. J.; Tully, J. C.; Kleyn, A. W. *J. Phys. Chem.* **1996**, *100*, 13021.
(15) D'Evelyn, M. P.; Madix, R. J. *Surf. Sci. Rep.* **1984**, *3*, 413.
(16) Asscher, M.; Somorjai, G. A. In *Atomic and Molecular Beam Methods*; Scoles, G., Ed.; Oxford University Press: New York, 1988; Vol. 2, p 489.
(17) Barker, J. A.; Auerbach, D. J. *Surf. Sci. Rep.* **1985**, *4*, 1.
(18) Yu, M. L.; DeLouise, L. A. *Surf. Sci. Rep.* **1994**, *19*, 285.
(19) Becker, C.; Henry, C. R. *Surf. Sci.* **1996**, *352*, 457.
(20) Becker, C.; Henry, C. R. *Catal. Lett.* **1997**, *43*, 55.
(21) Duriez, C.; Henry, C. R.; Chapon, C. *Surf. Sci.* **1991**, *253*, 191.
(22) Henry, C. R.; Chapon, C.; Goyhenex, C.; Monot, R. *Surf. Sci.* **1992**, *272*, 283.
(23) Henry, C. R.; Chapon, C.; Duriez, C. *Z. Phys. D* **1991**, *19*, 347.
(24) Henry, C. R.; Chapon, C.; Duriez, C. *J. Chem. Phys.* **1991**, *95*, 804.
(25) Jungwirthova, I.; Stara, I.; Matolin, V. *Surf. Sci.* **1997**, *377*, 644.
(26) Matolin, V.; Stara, I. *Surf. Sci.* **1998**, *398*, 117.
(27) Nehasil, V.; Hrncir, T.; Zafeiratos, S.; Ladas, S.; Matolin, V. *Surf. Sci.* **2000**, *454*, 289.
(28) Nehasil, V.; Stara, I.; Matolin, V. *Surf. Sci.* **1996**, *352*, 305.
(29) Nehasil, V.; Stara, I.; Matolin, V. *Surf. Sci.* **1997**, *377*, 813.
(30) Piccolo, L.; Becker, C.; Henry, C. R. *Eur. Phys. J. D* **1999**, *9*, 415.
(31) Piccolo, L.; Becker, C.; Henry, C. R. *Appl. Surf. Sci.* **2000**, *164*, 156.
(32) Piccolo, L.; Henry, C. R. *Appl. Surf. Sci.* **2000**, *162−163*, 670.
(33) Piccolo, L.; Henry, C. R. *Surf. Sci.* **2000**, *452*, 198.
(34) Stará, I.; Gonzales, V.; Jungwirthova, I.; Masek, K.; Matolin, V. *Surf. Rev. Lett.* **1998**, *5*, 397.
(35) Stara, I.; Matolin, V. *Surf. Sci.* **1994**, *313*, 99.
(36) Stara, I.; Matolin, V. *Surf. Rev. Lett.* **1997**, *4*, 1353.
(37) Stará, I.; Nehasil, V.; Matolín, V. *Surf. Sci.* **1995**, *331−333*, 173.
(38) Stara, I.; Tomkova, E.; Matolin, V. *Czech. J. Phys.* **1993**, *43*, 1023.
(39) Libuda, J.; Meusel, I.; Hartmann, J.; Freund, H.-J. *Rev. Sci. Instrum.* **2000**, *71*, 4395.
(40) Dellwig, T.; Hartmann, J.; Libuda, J.; Meusel, I.; Rupprechter, G.; Unterhalt, H.; Freund, H.-J. *J. Mol. Catal. A* **2000**, *162*, 51.
(41) Meusel, I.; Hoffmann, J.; Hartmann, J.; Heemeier, M.; Bäumer, M.; Libuda, J.; Freund, H.-J. *Catal. Lett.* **2001**, *71*, 5.
(42) Libuda, J.; Meusel, I.; Hoffmann, J.; Hartmann, J.; Piccolo, L.; Henry, C. R.; Freund, H.-J. *J. Chem. Phys.* **2001**, *114*, 4669.
(43) Meusel, I.; Hoffmann, J.; Hartmann, J.; Libuda, J.; Freund, H.-J. *J. Phys. Chem. B* **2001**, *105*, 3567.
(44) Libuda, J.; Meusel, I.; Hoffmann, J.; Hartmann, J.; Freund, H.-J. *J. Vac. Sci. Technol. A* **2001**, *19*, 1516.
(45) Hoffmann, J.; Meusel, I.; Hartmann, J.; Libuda, J.; Freund, H.-J. *J. Catal.* **2001**, *204*, 378.
(46) Hoffmann, J.; Schauermann, S.; Hartmann, J.; Zhdanov, V. P.; Kasemo, B.; Libuda, J.; Freund, H.-J. *Chem. Phys. Lett.* **2002**, *354*, 403.
(47) Shaikhutdinov, S.; Heemeier, M.; Hoffmann, J.; Meusel, I.; Richter, B.; Bäumer, M.; Kuhlenbeck, H.; Libuda, J.; Freund, H.-J.; Oldman, R.; Jackson, S. D.; Konvicka, C.; Schmid, M.; Varga, P. *Surf. Sci.* **2002**, *501*, 270.
(48) DeLouise, L. A. *J. Chem. Phys.* **1991**, *94*, 1528.
(49) Rocca, M.; Valbusa, U.; Gussoni, A.; Maloberti, G.; Racca, L. *Rev. Sci. Instrum.* **1991**, *62*, 2172.
(50) Holmblad, P. M.; Wambach, J.; Chorkendorff, I. *J. Chem. Phys.* **1995**, *102*, 1.
(51) Bowker, M.; Pudney, P. D. A.; Barnes, C. J. *J. Vac. Sci. Technol. A* **1990**, *8*.
(52) Eldridge, B. N.; Yu, M. L. *Rev. Sci. Instrum.* **1987**, *58*, 1014.
(53) Gibson, K. D.; Sibener, S. J. *J. Chem. Phys.* **1988**, *88*, 791.
(54) Balooch, M.; Siekhaus, W. J.; Olander, D. R. *J. Phys. Chem.* **1984**, *88*, 3521.
(55) Pradere, F.; Chateau, M.; Benslimane, M.; Bierry, M.; Chatelet, M.; Clement, D.; Guilbaud, A.; Jeannot, J. C.; Martino, A. D.; Vach, H. *Rev. Sci. Instrum.* **1994**, *65*, 161.
(56) Comsa, G.; David, R. *Surf. Sci. Rep.* **1985**, *5*, 145.
(57) Gillet, E.; Channakhone, S.; Matolin, V.; Gillet, M. *Surf. Sci.* **1985**, *152/153*, 603.
(58) Stará, I.; Nehasil, V.; Matolín, V. *Surf. Sci.* **1996**, *365*, 69.
(59) King, D. A.; Wells, M. G. *Surf. Sci.* **1972**, *29*, 454.
(60) King, D. A.; Wells, M. G. *Proc. R. Soc. London, Ser. A* **1974**, *339*, 245.
(61) Engel, T. *J. Chem. Phys.* **1978**, *69*, 373.
(62) Engel, T.; Ertl, G. *J. Chem. Phys.* **1978**, *69*, 1267.
(63) Sandell, A.; Libuda, J.; Brühwiler, P. A.; Andersson, S.; Maxwell, A. J.; Bäumer, M.; Mårtensson, N.; Freund, H.-J. *J. Vac. Sci. Technol. A* **1996**, *14*, 1546.
(64) Yudanov, I. V.; Sahnoun, R.; Neyman, K. M.; Rösch, N. Unpublished.
(65) Hammer, B. *J. Catal.* **2001**, *199*, 171.
(66) Engel, T.; Ertl, G. In *The Chemical Physics of Solid Surfaces and Heterogeneous Catalysis*; King, D. A., Woodruff, D. P., Eds.; Elsevier: New York, 1982; Vol. 4, p 73.
(67) Campbell, C. T.; Ertl, G.; Kuipers, H.; Segner, J. *J. Chem. Phys.* **1980**, *73*, 5863.
(68) Brown, L. S.; Sibener, S. J. *J. Chem. Phys.* **1988**, *89*, 1163.
(69) Brown, L. S.; Sibener, S. J. *J. Chem. Phys.* **1989**, *90*, 2807.
(70) Colonell, J. I.; Gibson, K. D.; Sibener, S. J. *J. Chem. Phys.* **1995**, *103*, 6677.
(71) Wolter, K.; Seiferth, O.; Kuhlenbeck, H.; Bäumer, M.; Freund, H.-J. *Surf. Sci.* **1998**, *399*, 190.
(72) Frank, M.; Bäumer, M. *Phys. Chem. Chem. Phys.* **2000**, *2*, 4265.
(73) Hoffmann, F. M. *Surf. Sci. Rep.* **1983**, *3*, 107.
(74) Gieβel, T.; Schaff, O.; Hirschmugl, C. J.; Fernandez, V.; Schindler, K.-M.; Theobald, A.; Bao, S.; Lindsay, R.; Berndt, W.; Bradshaw, A. M.; Baddeley, C.; Lee, A. F.; Lambert, R. M.; Woodruff, D. P. *Surf. Sci.* **1998**, *406*, 90.
(75) Zhdanov, V. P.; Kasemo, B. *Surf. Sci. Rep.* **2000**, *39*, 25.
(76) Seebauer, E. G.; Allen, C. E. *Prog. Surf. Sci.* **1995**, *49*, 265.
(77) Wintterlin, J. *Adv. Catal.* **2001**, *45*, 131.
(78) Wintterlin, J.; Völkening, S.; Janssens, T. V. W.; Zambelli, T.; Ertl, G. *Science* **1997**, *278*, 1931.
(79) Huang, W.; Zhai, R.; Bao, X. *Langmuir* **2001**, *17*, 3629.
(80) Matsushima, T.; Asada, H. *J. Chem. Phys.* **1986**, *85*, 1658.
(81) Frank, M.; Bäumer, M. Private communication.